Quadratic extension to retrace error calibration algorithm for non-null interferometric surface figure testing of nominally flat reflective surfaces

Martin Tangari Larrategui[1,2], Yanqi Zhang [2], Andrew D. Rocha, Thomas G. Brown [1], and Jonathan D. Ellis [2]
1 University of Rochester, Rochester, NY 14627, USA
2 University of Arizona, Tucson, AZ 85721, USA
Correspondence: mtangari@ur.rochester.edu

Abstract: We present a slope dependent calibration algorithm for interferometric surface figure testing. RMS wavefront error is reduced 40.7% (10.8% for linear method) from the uncalibrated measurement for a R/22.7 mirror tested against a flat reference. © 2019 The Author(s)
OCIS codes: 110.0110 Imaging systems; 120.0120 Instrumentation, measurement, and metrology

1. Introduction

Proper calibration is a key attribute of non-null surface figure testing interferometers. The distinct path travelled by the test and reference rays leads to systematic non-common path (retrace) errors in the phase measurement [1]. These retrace errors cannot be neglected when working with dual wavelength interferometry or other methods that extend the interferometer's dynamic range well beyond the monochromatic Nyquist limit [2]. To counteract this, an example calibration method was patented by Dörband and Frank [3] and published in the literature by Dörband et al. [4]. Their algorithm assumes long range retrace errors (caused by aberrations in the imaging lens and misalignments) to be linearly dependent on the slope departure of the test surface.

The Dörband and Frank linear calibration method and our proposed extension were tested in FRED using a pair of 1:1 stock optics relay lenses individually color corrected for 594 and 604 nm wavelengths. The lenses were designed to test surfaces of up to 1.4° of slope departure and 11 mm diameter and have a maximum wavefront error RMS of 0.02 waves across the field for both wavelengths. The imaging lens is shown in Figure 1.

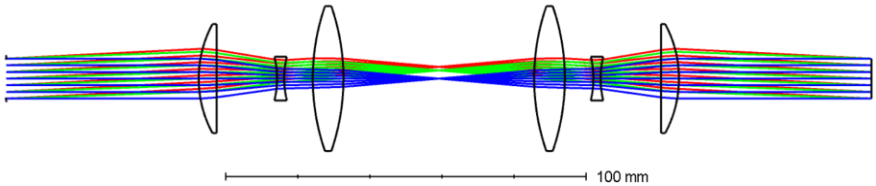

Fig. 1. A 1:1 relay imaging lens composed of a pair of stock optics Cooke Triplets. The test and reference surfaces are modelled as the aperture stop/entrance pupil, which are imaged to the detector (exit pupil) [5].

2. Linear and quadratic calibration

For the linear algorithm, the phase error across the pupil is measured for two flat calibration surfaces tilted by the maximum interferometer acceptance angle along two orthogonal directions ($\alpha_x = \alpha_y = \alpha_{MAX}$, half the imaging lens HFOV). For unity magnification, the calibration to be applied at each (x, y) pupil point is given by [3, 4]

$$C(x,y) = \frac{E_C\left(x,y,\alpha_x,\alpha_y\right)\Big|_{\substack{\alpha_x=\alpha_{MAX}\\ \alpha_y=0}}}{\alpha_{MAX}} \arctan\left(\frac{\partial Z(x,y)}{\partial x}\right) + \frac{E_C\left(x,y,\alpha_x,\alpha_y\right)\Big|_{\substack{\alpha_x=0\\ \alpha_y=\alpha_{MAX}}}}{\alpha_{MAX}} \arctan\left(\frac{\partial Z(x,y)}{\partial y}\right), \quad (1)$$

where $E_C(x, y, \alpha_x, \alpha_y)$ is the phase measurement error (phase measurement minus the ideal phase for the calibration input tilt) at the two extrema angles. The linear assumption is usually appropriate for null and quasi-null monochromatic surface figure testing where the maximum departure angle is constrained to a small value by the Nyquist limit but large enough to be significant (>10λ) [3]. For larger departures of non-null interferometry, the effects of higher order terms cannot be disregarded. Assuming all odd power order errors are linear and all even power errors are quadratic in slope departure, the calibration function can be extended to second order using

$$
\begin{aligned}
C(x,y) = {} & \frac{1}{2\alpha_{MAX}}\left(E_C(x,y,\alpha_x,\alpha_y)\Big|_{\substack{\alpha_x=\alpha_{MAX}\\ \alpha_y=0}} - E_C(x,y,\alpha_x,\alpha_y)\Big|_{\substack{\alpha_x=-\alpha_{MAX}\\ \alpha_y=0}} \right)\arctan\left(\frac{\partial Z(x,y)}{\partial x}\right) \\
& + \frac{1}{2\alpha_{MAX}}\left(E_C(x,y,\alpha_x,\alpha_y)\Big|_{\substack{\alpha_x=0\\ \alpha_y=\alpha_{MAX}}} - E_C(x,y,\alpha_x,\alpha_y)\Big|_{\substack{\alpha_x=0\\ \alpha_y=-\alpha_{MAX}}} \right)\arctan\left(\frac{\partial Z(x,y)}{\partial y}\right) \\
& + \frac{1}{2(\alpha_{MAX})^2}\left(E_C(x,y,\alpha_x,\alpha_y)\Big|_{\substack{\alpha_x=\alpha_{MAX}\\ \alpha_y=0}} + E_C(x,y,\alpha_x,\alpha_y)\Big|_{\substack{\alpha_x=-\alpha_{MAX}\\ \alpha_y=0}} \right)\left(\arctan\left(\frac{\partial Z(x,y)}{\partial x}\right)\right)^2 \\
& + \frac{1}{2(\alpha_{MAX})^2}\left(E_C(x,y,\alpha_x,\alpha_y)\Big|_{\substack{\alpha_x=0\\ \alpha_y=\alpha_{MAX}}} + E_C(x,y,\alpha_x,\alpha_y)\Big|_{\substack{\alpha_x=0\\ \alpha_y=-\alpha_{MAX}}} \right)\left(\arctan\left(\frac{\partial Z(x,y)}{\partial y}\right)\right)^2 \\
& + \frac{1}{4(\alpha_{INT})^2}\left(E_C(x,y,\alpha_x,\alpha_y)\Big|_{\substack{\alpha_x=\alpha_{INT}\\ \alpha_y=\alpha_{INT}}} + E_C(x,y,\alpha_x,\alpha_y)\Big|_{\substack{\alpha_x=-\alpha_{INT}\\ \alpha_y=-\alpha_{INT}}} \right)\arctan\left(\frac{\partial Z(x,y)}{\partial x}\right)\arctan\left(\frac{\partial Z(x,y)}{\partial y}\right) \\
& - \frac{1}{4(\alpha_{INT})^2}\left(E_C(x,y,\alpha_x,\alpha_y)\Big|_{\substack{\alpha_x=\alpha_{INT}\\ \alpha_y=-\alpha_{INT}}} + E_C(x,y,\alpha_x,\alpha_y)\Big|_{\substack{\alpha_x=-\alpha_{INT}\\ \alpha_y=\alpha_{INT}}} \right)\arctan\left(\frac{\partial Z(x,y)}{\partial x}\right)\arctan\left(\frac{\partial Z(x,y)}{\partial y}\right),
\end{aligned}
\tag{2}
$$

where α_{INT} is the maximum tilt angle in an orthogonal basis rotated by 45° with respect to the (α_x, α_y) basis. The eight phase error measurements required for this extended calibration measurement are shown in Figure 2. The performance of each calibration algorithm for a 11 mm diameter, 250 mm radius of curvature concave mirror is shown in Figure 3.

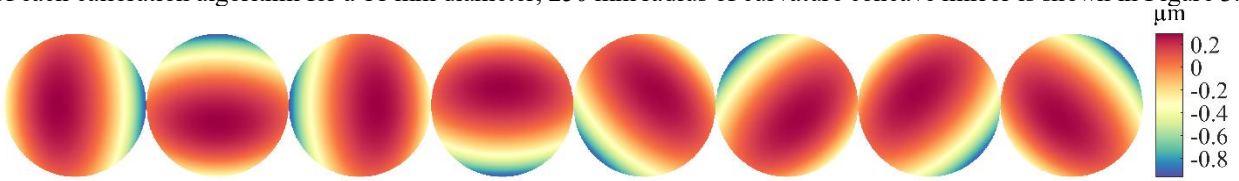

Fig. 2. Phase error measurements for tilted flat calibration surfaces. From left to right: (α_{MAX}, 0), (0, α_{MAX}), (-α_{MAX},0), (0, -α_{MAX}), (-α_{INT}, -α_{INT}), (-α_{INT}, α_{INT}), (α_{INT}, -α_{INT}), and (α_{INT}, α_{INT}). The limiting aberrations are tilt (linear in slope departure), astigmatism and field curvature (quadratic in slope departure). Only the first two phase error measurements are used for the linear method existing in the literature [3,4].

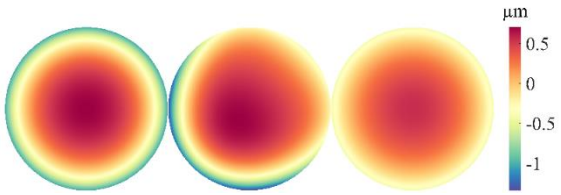

Fig. 3. Test surface sag measurement error. From left to right: before calibration (1.75 µm PV, 1.57 µm RMS), after linear calibration (2.05 µm PV, 1.40 µm RMS) and after second order calibration (1.00 µm PV, 0.93 µm RMS).

3. Conclusion

The linear calibration algorithm provides inaccurate results when second and higher order errors become non-negligible, leading to better performance for points with slope departures close to the calibration values and worse performance for the rest of the pupil. The extension to second order solves this problem. Future research will focus on extending this method to higher orders and decoupling the slope dependent monochromatic error from the chromatically magnified dual wavelength errors.

4. References

[1] N. Gardner and A. Davies, "Retrace error evaluation on a figure-measuring interferometer," Proc. SPIE **5869**, 58690V (2005)
[2] Y.-Y. Cheng and J.C. Wyant, "Two-wavelength phase shifting interferometry," Appl. Opt. **23**, 4539-4543 (1984)
[3] B. Dörband and R. Frank, Method and an apparatus for measuring a deviation of an optical test surface from a target shape, U.S. Patent No. 8269981 B1 (2012).
[4] Dörband B., Müller H. and Gross H., "Testing the Geometry of Optical Components" in *Handbook of optical systems: Volume 5: Metrology of optical components and systems,* (WILEY-VCH Verlag GmbH 2012), pp. 745-747.
[5] P.E. Murphy, T.G. Brown, and D.T. Moore, "Interference imaging for aspheric surface testing," Appl. Opt. **39**, 2122-2129 (2000)